Desalination and Water Treatment
www.deswater.com
doi: 10.1080/19443994.2014.940658

55 (2015) 3218–3230
September

Taylor & Francis
Taylor & Francis Group

Numerical study of flow, temperature, and salinity distributions of a brine discharge problem

Sami Al-Sanea, Jamel Orfi*, Abdullah Najib

Mechanical Engineering Department, College of Engineering, King Saud University, P.O. Box 800, Riyadh 11421, KSA, Tel. +966 11 467 9798; Fax: +966 11 467 6652; email: orfij@ksu.edu.sa (J. Orfi)

Received 1 April 2014; Accepted 16 June 2014

ABSTRACT

In this study, the problem of brine discharge into sea is studied numerically. A 3D model for the heat and brine dispersion in the vicinity of discharge and intake ports is developed using *Fluent* package. The flow is taken turbulent and the fluid properties are considered variable with salinity and temperature. The results are expressed in terms of streamlines, isotherms, and salinity contours as well as velocity, temperature, and salinity profiles. These results give the excess temperature and salinity relative to the nominal values of the free stream. Effect of discharge mass flow rate on patterns of temperature and salinity contours is presented and analyzed. It is observed in particular that for the different simulations undertaken, the excess temperature and salinity can be important and the intake is always affected by the discharge conditions.

Keywords: Brine discharge; Numerical modeling; Shallow water; Dispersion; Heat and mass transfer

1. Introduction

The discharge to the environment of huge amounts of highly concentrated saline water with relatively high temperature is one of the major problems associated with the desalination industry. An exhaustive review on environmental impacts resulting from brine discharge problems can be found in Bleninger and Jirka [1]. Results were reported from available monitoring and laboratory studies. It was observed that the majority of studies had focused on a limited number of species over a short period of time with no baseline data; the need for a more uniform assessment and monitoring approach was underlined. Besides, the authors presented environmental standards for temperature, salinity, and residual chemicals as well as regulations on mixing zones.

In addition, the effluent contains additives such as chemicals used for bio-fouling control and anti-scalants as well as corrosion products. Several studies analyzed the chemical aspects of brine discharge and impacts on the marine environment (see e.g. Ahmed et al. [2] and Danoun [3]). Al Mutaz [4] and Abdul Azis et al. [5] discussed impact of effluents from Saudi desalination plants in Jeddah and Al-Jubail desalination plants, respectively.

*Corresponding author.

Presented at the Conference on Desalination for the Environment: Clean Water and Energy 11–15 May 2014, Limassol, Cyprus

A procedure for environmental impact assessment for desalination plants was proposed by Hoepner [6], while Alameddine and El-Fadel [7] adopted discharge assessment methodology consisting of six phases. Muñoz and Fernández-Alba [8] presented a life cycle assessment methodology and showed that reverse osmosis desalination could significantly reduce its environmental impact if, instead of seawater resources, brackish groundwater resources were used. Sommariva et al. [9] presented a simple mathematical model, based on mass and energy balance, to assess thermal impact on the external environment by a desalination plant of different capacities and performances.

Methods for brine rejection can be divided into two classes depending on whether the desalination plants are inland (evaporation pond method) or coastal (surface water discharge method). Alameddine and El-Fadel [7] performed a comparison study of advantages and disadvantages of various brine disposal options and presented design recommendations for brine discharge. Bleninger and Jirka [1] discussed the "zero liquid discharge" method which has the potential to provide freshwater without any brine discharges and impacts on the marine environment.

There are several physical phenomena occurring during brine discharge into surface water bodies, e.g. the sea. Dispersion, diffusion, convection, and buoyancy are the main ones. The discharge process can be divided into two different regions depending on the relative magnitude of the physical phenomena involved. The first region, known as the near field region, is situated in the vicinity of the outfall systems. The second region, known as the far field region, is determined by ambient transport mechanisms such as ambient diffusion and advection [10,11]. An intermediate field separating the near and far fields can also be considered. The design of the outfall characteristics including the diffusers is an essential parameter in achieving the efficient possible dilution in the near field. Bleninger et al. [10] characterized two important elements of brine discharge process. The first element is related to the discharge characteristics while the second element concerns the receiving water characteristics which are determined by the local site conditions and the regional conditions. Bleninger [11] stated that the main problems in discharge process occur due to limited mixing behavior in the receiving waters. Thus, in order to reduce such problems, it is important to enhance effluent dispersion in the receiving water and adequate discharge sitting to avoid pollutant accumulation.

In shallow coastal waters, the effluent is commonly discharged through open channels located on the shoreline in which variations of the effluent velocity, salinity, and temperature over the depth are practically negligible. The discharged effluent can, therefore, be assumed to be well mixed over the water depth. Shallow water mathematical modeling of such discharges accounts for these distinguishing features. Among the classical and pioneering studies in which mathematical modeling of free surface flows has been explained comprehensively are those of Kuipers and Vreugdenhil [12], Spalding [13], and Rodi [14]. Kuipers and Vreugdenhil [12] presented a detailed account on the nature of shallow water flows and the derivation of the depth-averaged equations. Al-Sanea [15] developed a finite-volume numerical procedure for the calculation of 2D depth-integrated shallow-water flows. Subsequently, Al-Sanea [16] developed a numerical model accounting for the physical features that affect the concentrated brine dispersion process including: the convective and diffusive transport, wind stresses, seabed friction, and variable seabed elevation.

More recent studies include those of Purnalna et al. and Purnama and Al-Barwani [17,18], Shao et al. [19] and Purnama and Al-Barwani [20]. Purnalna et al. [17] used an analytical model to solve the transient salinity diffusion–advection equation in order to investigate dispersion of brine waste discharges into sea. Purnama and Al-Barwani [20] solved the 2D advection–diffusion equation for salt concentration to investigate the effect of a tidally oscillating flow in dispersing brine waste discharge into sea. The geometry was simplified using a straight coast with a constant water depth. Al-Barwani and Purnama [21] studied the effect of beach erosion on dispersing the brine waste discharged into sea.

A number of studies have used the Cornel Mixing Zone Expert System *Cormix* developed by Jirka and co-authors. The system provides comprehensive approach to mixing zone analysis, regulatory assessment, and outfall design (Donecker and Jirka [22]). Alameddine and El-Fadel [7] used the *Cormix* model to simulate dispersion of brine plume in marine environment by considering the heated effluent from a desalination power plant in the Arabian Gulf region. The authors highlighted several limitations of the *Cormix* model including its limited capability for simulating the discharge of large flow volumes in shallow areas.

Malcangio and Petrillo [23] used a 3D model to simulate brine discharge from desalination plants in a coastal region in the south of Italy characterized by the presence of protected vegetation species. The Reynolds Averaged Navier–Stokes equations were considered and data on topography of target area and climatic conditions were introduced in the model.

Results in terms of excess salinity were analyzed and the most suitable location for the brine outfall was determined.

Palomar and Losada [24] discussed and compared three basic approaches for modeling the impact of brine discharge on the marine environment. These are: (1) models based on a dimensional analysis of the phenomenon, (2) models based on integration of differential equations along the cross-section of flow, and (3) hydrodynamic models.

Palomar et al. [25] examined modeling of near field brine discharge and analyzed assumptions, capability, limitations, and reliability of steady-state models that are used. These models were either based on dimensional analysis such as *Cormix* or based on integration of differential equations such as *Corjet*, *Visual Plumes*, and *Visjet*. The authors observed a major common shortcoming in these commercial models which was the lack of validation studies for negatively buoyant jets. Some significant errors were detected in the sensitivity analysis that was carried out. Palomar et al. [26] focused on the validation of these models via performing many tests simulating different cases and using available published experimental data.

A simple model for simulating behavior of dense jets was developed by Cipollina et al. [27]. The model considered four basic jet parameters; namely, flow rate, density, inclination, and diameter. Results included information on trajectory, spreading, and dilution of inclined dense jets. Abou-Elhaggag et al. [28] investigated jet trajectory and dilution of submerged negatively buoyant jet discharging vertically over a flat bottom in a calm ambient environment. Experimental observations made for terminal height of rise of dense jets and for concentration profiles along jet trajectory were used to validate a numerical model using *Fluent* package. Loya-Fernández et al. [29] studied the accuracy of four mixing zone models by conducting a comparative study with brine discharge measurements from a reverse osmosis desalination plant in Spain. Very recently, Oliver et al. [30] developed an integral model to predict the near field behavior of negatively buoyant discharges in quiescent ambient fluid. The model included influences of additional mixing associated with buoyancy-induced instabilities. Comparisons were carried out with predictive models and experimental data.

Environmental impacts of seawater desalination plants are related mainly to heated and concentrated brine discharges into receiving water bodies. Several studies considered the brine and heat dispersion modeling but the majority adopted simplified approaches with various limiting assumptions. Therefore, much more work is needed in this field.

The purpose of this paper is to present a 3D numerical model for predicting brine and heat dispersion into shallow waters. The model expresses the conservation equations of mass, momentum, species, and temperature. Turbulence is accounted for by employing the standard k-ε model of turbulence and the commercial CFD *Fluent* package is used. Results of a parametric study are presented for a hypothetical discharge problem.

2. Mathematical formulation

The discharge problem under consideration can be simplified and represented schematically as given in Fig. 1. The discharge and intake ports are assumed to be located on the shoreline and are 200 m apart. The depth profile is linear with a slope of 1.8% and is taken at coastline equal to 2 m. The other dimensions related to this 3D configuration are summarized in Table 1. The x, y, and z coordinates refer to the width, depth, and length, respectively. A parametric study is performed to investigate the flow, temperature, and

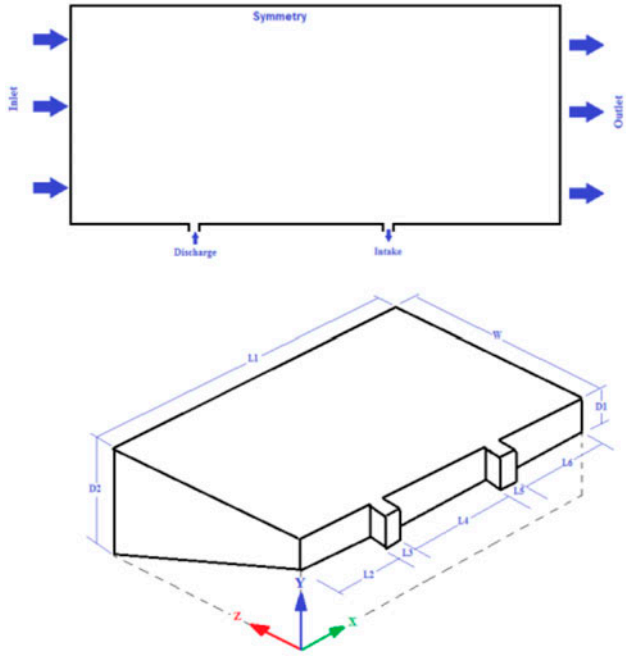

Fig. 1. Schematic representation of the physical model.

Table 1
Dimensions related to the 3D configuration

Dimension	*L*1	*L*2	*L*3	*L*4	*L*5	*L*6	*W*	*D*1	*D*2
Value (m)	500	100	5	200	5	190	250	2	10

salinity distributions and the effects of discharge on the intake conditions for various discharge mass flow rates and various sea current velocities.

2.1. Basic equations

The governing equations are those of conservation of mass, energy, and species expressed in rectangular 3D coordinates. Steady-state conditions are considered, while the fluid properties are taken as variable with salinity and temperature. The standard k-ε model implemented in *Fluent* software [31] is chosen to account for the turbulence character of the flow. The wind effects are neglected as well the evaporation at the air–water interface. The sea current velocity is taken constant and uniform.

The governing equations for the case of 3D configuration are as follows [31]:

- Continuity equation

$$\frac{\partial \rho}{\partial t}+\frac{\partial}{\partial x}(\rho u)+\frac{\partial}{\partial y}(\rho v)+\frac{\partial}{\partial z}(\rho w)=0$$

- Momentum equation

Momentum equation in x-direction

$$\frac{\partial \rho u}{\partial t}+\frac{\partial}{\partial x}(\rho uu)+\frac{\partial}{\partial y}(\rho vu)+\frac{\partial}{\partial z}(\rho wu) = \rho g_x-\frac{\partial P}{\partial x}+\frac{\partial}{\partial x}\left(\mu_e\frac{\partial u}{\partial x}\right)+\frac{\partial}{\partial y}\left(\mu_e\frac{\partial u}{\partial y}\right)+\frac{\partial}{\partial z}\left(\mu_e\frac{\partial u}{\partial z}\right)+R_x+T_x$$

Momentum equation in y-direction

$$\frac{\partial \rho v}{\partial t}+\frac{\partial}{\partial x}(\rho uv)+\frac{\partial}{\partial y}(\rho vv)+\frac{\partial}{\partial z}(\rho wv) = \rho g_y-\frac{\partial P}{\partial y}+\frac{\partial}{\partial x}\left(\mu_e\frac{\partial v}{\partial x}\right)+\frac{\partial}{\partial y}\left(\mu_e\frac{\partial v}{\partial y}\right)+\frac{\partial}{\partial z}\left(\mu_e\frac{\partial v}{\partial z}\right)+R_y+T_y$$

Momentum equation in z-direction

$$\frac{\partial \rho w}{\partial t}+\frac{\partial}{\partial x}(\rho uw)+\frac{\partial}{\partial y}(\rho vw)+\frac{\partial}{\partial z}(\rho ww) = \rho g_z-\frac{\partial P}{\partial z}+\frac{\partial}{\partial x}\left(\mu_e\frac{\partial w}{\partial x}\right)+\frac{\partial}{\partial y}\left(\mu_e\frac{\partial w}{\partial y}\right)+\frac{\partial}{\partial z}\left(\mu_e\frac{\partial w}{\partial z}\right)+R_z+T_z$$

where the terms T_x, T_y, and T_z are viscous loss terms which are eliminated in the incompressible, constant property case. They are expressed respectively as:

$$T_x=\frac{\partial}{\partial x}\left(\mu\frac{\partial u}{\partial x}\right)+\frac{\partial}{\partial y}\left(\mu\frac{\partial v}{\partial x}\right)+\frac{\partial}{\partial z}\left(\mu\frac{\partial w}{\partial x}\right)$$

$$T_y=\frac{\partial}{\partial x}\left(\mu\frac{\partial u}{\partial y}\right)+\frac{\partial}{\partial y}\left(\mu\frac{\partial v}{\partial y}\right)+\frac{\partial}{\partial z}\left(\mu\frac{\partial w}{\partial y}\right)$$

$$T_z=\frac{\partial}{\partial x}\left(\mu\frac{\partial u}{\partial z}\right)+\frac{\partial}{\partial y}\left(\mu\frac{\partial v}{\partial z}\right)+\frac{\partial}{\partial z}\left(\mu\frac{\partial w}{\partial z}\right)$$

- Energy equation

$$\frac{\partial}{\partial t}(\rho CpT_o)+\frac{\partial}{\partial x}(\rho uCpT_o)+\frac{\partial}{\partial y}(\rho vCpT_o)+\frac{\partial}{\partial z}(\rho wCpT_o) = \frac{\partial}{\partial x}\left(k\frac{\partial T_o}{\partial x}\right)+\frac{\partial}{\partial y}\left(k\frac{\partial T_o}{\partial y}\right)+\frac{\partial}{\partial z}\left(k\frac{\partial T_o}{\partial z}\right)+W^v+E^k+Q_v+\Phi+\frac{\partial P}{\partial t}$$

where C_p and k are the specific heat and the thermal conductivity; T_o refers to the total (or stagnation) temperature expressed as function of the static temperature as: $T+V^2/2C_p$; V is the magnitude of the velocity vector; W^v is the viscous work term; Q_v is the volumetric heat source; Φ is viscous heat generation term; and E^k refers to the kinetic energy.

Species transport

$$\frac{\partial \rho S}{\partial t}+\frac{\partial}{\partial x}(\rho uS)+\frac{\partial}{\partial y}(\rho vS)+\frac{\partial}{\partial z}(\rho wS)=-\nabla.\vec{J}+S_s$$

with

$$\vec{J}=-\left(\rho D_m+\frac{\mu_t}{Sc_t}\right)\nabla S-D_s\nabla T\frac{\nabla T}{T}$$

where Sc_t is the turbulent Schmidt number ($\mu_t/\rho D_t$ where μ_t is the turbulent viscosity and D_t is the turbulent diffusivity). The default Sc_t is 0.7. Note that turbulent diffusion generally overwhelms laminar diffusion, and the specification of detailed laminar diffusion properties in turbulent flows is generally not necessary. D_m is the mass diffusion coefficient and D_s is the thermal (Soret) diffusion coefficient. S_s represents the source term in the mass transfer equation.

- *Standard k–ε turbulence model*

$$\frac{\partial}{\partial t}(\rho\kappa)+\frac{\partial}{\partial x}(\rho u\kappa)+\frac{\partial}{\partial y}(\rho v\kappa)+\frac{\partial}{\partial z}(\rho w\kappa)=\left[\frac{\partial}{\partial x}\left(\frac{\mu_t}{\sigma_k}\frac{\partial\kappa}{\partial x}\right)+\frac{\partial}{\partial y}\left(\frac{\mu_t}{\sigma_k}\frac{\partial\kappa}{\partial y}\right)+\frac{\partial}{\partial z}\left(\frac{\mu_t}{\sigma_k}\frac{\partial\kappa}{\partial z}\right)+\mu_t\phi-\rho\varepsilon+\frac{C_4\beta\mu_t}{\sigma_t}\left(g_x\frac{\partial T}{\partial x}+g_y\frac{\partial T}{\partial y}+g_z\frac{\partial T}{\partial z}\right)\right]$$

$$\frac{\partial}{\partial t}(\rho\varepsilon)+\frac{\partial}{\partial x}(\rho u\varepsilon)+\frac{\partial}{\partial y}(\rho v\varepsilon)+\frac{\partial}{\partial z}(\rho w\varepsilon)=\left[\frac{\partial}{\partial x}\left(\frac{\mu_t}{\sigma_\varepsilon}\frac{\partial\varepsilon}{\partial x}\right)+\frac{\partial}{\partial y}\left(\frac{\mu_t}{\sigma_\varepsilon}\frac{\partial\varepsilon}{\partial y}\right)+\frac{\partial}{\partial z}\left(\frac{\mu_t}{\sigma_\varepsilon}\frac{\partial\varepsilon}{\partial z}\right)+C_{1\varepsilon}\mu_t\frac{\varepsilon}{\kappa}\varphi-C_2\rho\frac{\varepsilon^2}{\kappa}+\frac{C_\mu(1-C_3)\beta\rho\kappa}{\sigma_t}\left(g_x\frac{\partial T}{\partial x}+g_y\frac{\partial T}{\partial y}+g_z\frac{\partial T}{\partial z}\right)\right]$$

where T is temperature; S is mass fraction (salinity); V is the vector velocity; u, v, and w are velocity components; ρ, μ, k, and C_p are respectively the sea water density, dynamic viscosity, thermal conductivity, and specific heat; D is the mass diffusion coefficient; g_x, g_y, and g_z are the gravity components; R_x, R_y, and R_z account for the source term components, not considered here; μ_e is effective viscosity of flow; κ is turbulent kinetic energy; ε is turbulent kinetic energy dissipation rate; μ_t is the turbulent viscosity of flow; $C_{1\varepsilon}$, C_2, C_3, and C_4 are constants; C_μ is turbulence constant; σ_k, σ_ε, and σ_t are the turbulent Prandtl numbers; and β is thermal expansion. The constants in k–ε turbulence model equations are given in Table 2.

2.2. Boundary conditions

At the inlet of the domain, the velocity components are set equal to the sea current velocity components: $u=u_0$; $v_0=w_0=0$. One value of u_0 was considered here 0.05 m/s. The inlet temperature and salinity are set equal to those of the seawater: $T=T_0=300$ K, $S=S_0=4\%$ (40,000 ppm). The turbulence intensity is set to be equal to 2% and the hydraulic diameter equal to 4 m.

At the outlet of the domain, the pressure outlet condition was selected and used in the modeling.

Table 2
Constants in k-ε turbulence model equations

$\mu_t=\rho C_\mu k^2/\varepsilon$	$C_\mu=0.09$	$C_{1\varepsilon}=1.44$	$C_2=1.92$	$C_3=1.0$
$C_4=0.0$	$\sigma_k=1.0$	$\sigma_\varepsilon=1.3$	$\sigma_t=0.85$	$\beta=0.0$

The symmetry conditions apply far from the shoreline.

At the discharge port, the mass low rate, temperature, and salinity are supposed fixed. Three values of the mass flow rate are used in the computations: 1,000, 3,000, and 5,000 kg/s. The discharge temperature and salinity are respectively 313 K and 8%. The turbulence intensity is set to be equal to 2% and the hydraulic diameter equal to 4 m.

At the intake port, the mass flow rate is taken as double of the discharge mass flow rate, while the pressure outlet condition as described in *Fluent* package is selected.

At the coastline, the non slip and impermeable wall conditions apply. The temperature gradient is zero.

At the air–water interface, the normal gradients of the velocity, temperature, and salinity are considered equal to zero.

At the sea bed, the non slip and non moving wall conditions are used while the normal gradients of temperature and salinity are considered equal to zero.

2.3. Numerical model

To solve the above governing equations and boundary conditions, the *Fluent* software [31] was used. The algebraic forms of transport equations were achieved through the finite volume discretization. The upwind scheme is used to approximate the velocities at the faces of the control volumes. The variability of the sea water properties with the temperature and salinity was taken into account. Therefore, and due to limitation of the solver, a special treatment consisting of defining external functions expressing the seawater properties was incorporated in the *Fluent* code.

Appropriate mesh distribution was first generated. The grid distribution is not uniform: it is refined in the critical regions, where the variations of the computed variables (i.e. velocity components, temperature and salinity) are expected to be significant. Figs. 2(a) and 2(b) report the results of a grid independence analysis involving three different mesh sizes. The coarse mesh (Mesh1) consists of 225,000 nodes ($15\times75\times200$ in the depth, width and length respectively). The second one (Mesh2) has 700,000 ($20\times100\times350$) while the third one (Mesh3) has 1,875,000 nodes ($25\times150\times500$). Fig. 2(a) and 2(b) show that the distributions of the velocity magnitude and salinity profiles along the width and the depth, respectively, for the grid size of 700,000 nodes are practically the same as those for the case with 1,875,000 nodes. Therefore, the total number of nodes used in the present simulations for this 3D configuration is 700,000. A convergence

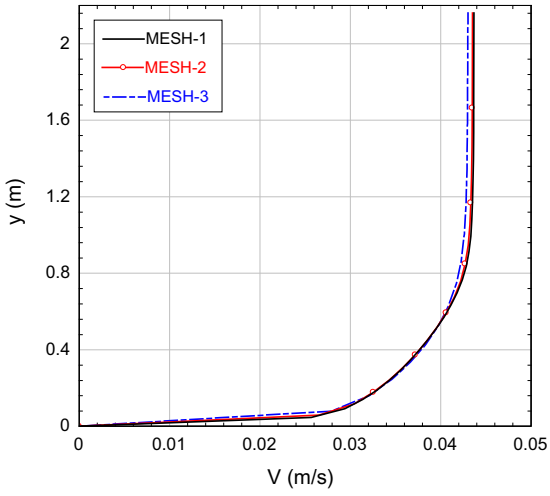

Fig. 2a. Distribution of the velocity profile along the depth for different grid sizes.

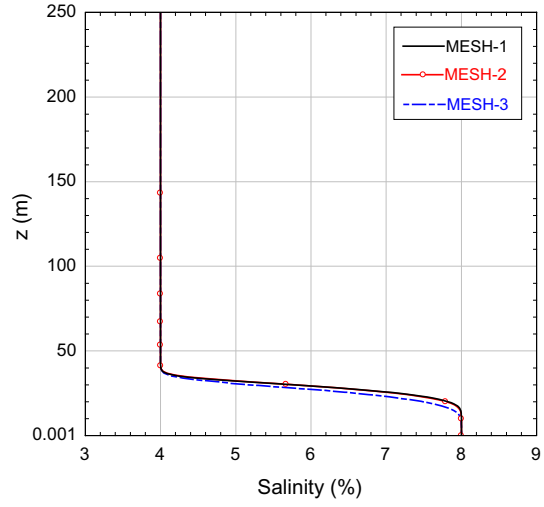

Fig. 2b. Distribution of the salinity profile along the width for different grid sizes.

criterion of 10^{-4} was imposed on the residuals of the continuity, momentum, energy, and species equations. Besides, the overall mass and energy balances were verified for each simulation.

On the other hand, some preliminary calculations for basic cases confirmed the accuracy and the capability of the numerical model to compute reliable results for the brine discharge problem under study. For example, we considered the case where the discharge salinity (temperature) was equal to the nominal salinity (temperature), the converged solution gave a uniform distribution of the salinity (temperature) equal to the seawater salinity (temperature).

3. Results and discussion

There are two main desalination processes: Multi stage flash (MSF) and reverse osmosis (RO). The rejected brine from MSF plants can have a temperature of 12°C higher than the ambient seawater. While for RO plants, there is no significant excess of temperature. On the other side, the recovery ratio of a desalination plant defined as the mass flow rate of the product to the feed mass flow rate can be around 60% for RO and 10–20% for MSF plants. Thus, the brine flows can be considerably large generally up to 40% for RO and up to 90% for MSF (including cooling water) [10].

In order to investigate the flow, temperature, and salinity distribution in the vicinity of the discharge and intake ports of a desalination plant, several simulations corresponding to different combinations

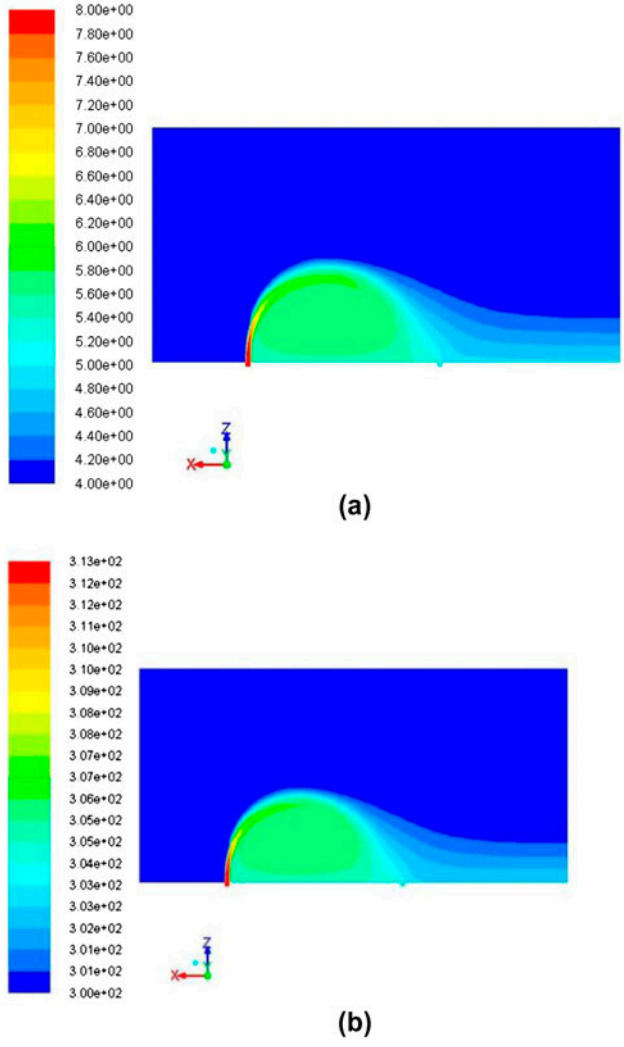

Fig. 3. Salinity (a) and temperature (b) contours at the free surface of the domain.

of discharge mass flow rates, temperature and salinity, and sea current velocity are performed. In the following, some of the obtained results are presented and discussed. The discharge salinity and temperature as well as the sea current velocity are kept constant at 8%, 313 K, and 0.05 m/s, respectively, while the discharge mass flow rate is varied. Three values of discharge mass flow rate are considered as 1,000, 3,000, and 5,000 kg/s.

3.1. General description

Fig. 3 depict the concentration contours and isotherms corresponding to the case where the discharge mass flow rate equals to 3,000 kg/s and the sea current velocity is 0.05 m/s. The computed contours show the significant influence of the flow patterns on the thermal and salinity fields. One can see that the domain is divided in two regions. The first region, located in the vicinity of the discharge and intake ports, is characterized by large variations of the temperature and the salinity values due to the recirculating flow structure. The second region, far from the discharge and intake ports, envelops the first region with the recirculation zone and extends to the entry and exit regions of the physical domain. The salinity and temperature are equal to the free stream values 4% and 300 K, respectively.

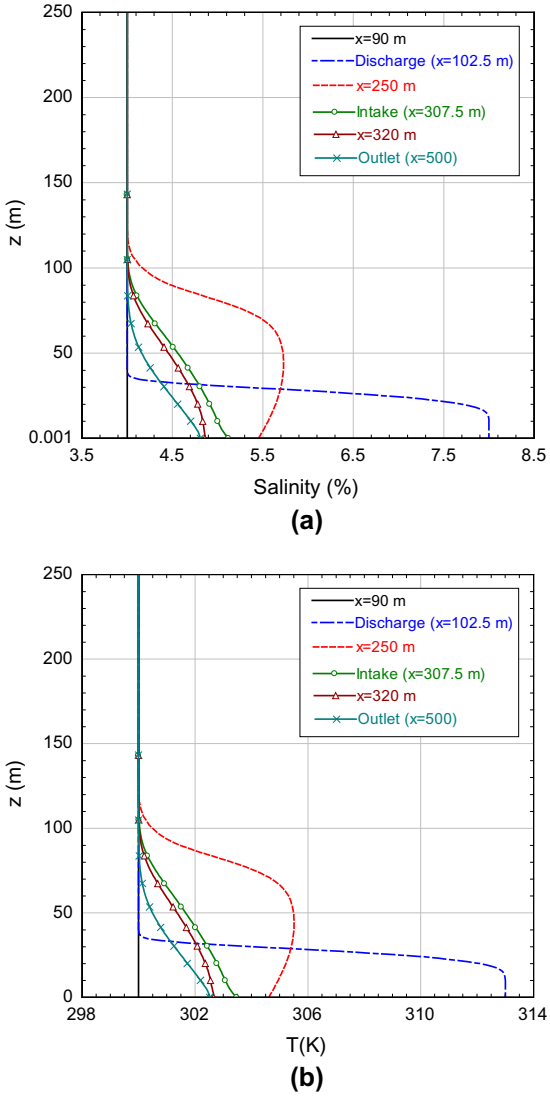

Fig. 4. Salinity (a) and temperature (b) profiles at different axial locations ($x = 90$ m, $x = 102.5$ m, $x = 250$ m, $x = 307.5$ m, $x = 320$ m and $x = 500$ m).

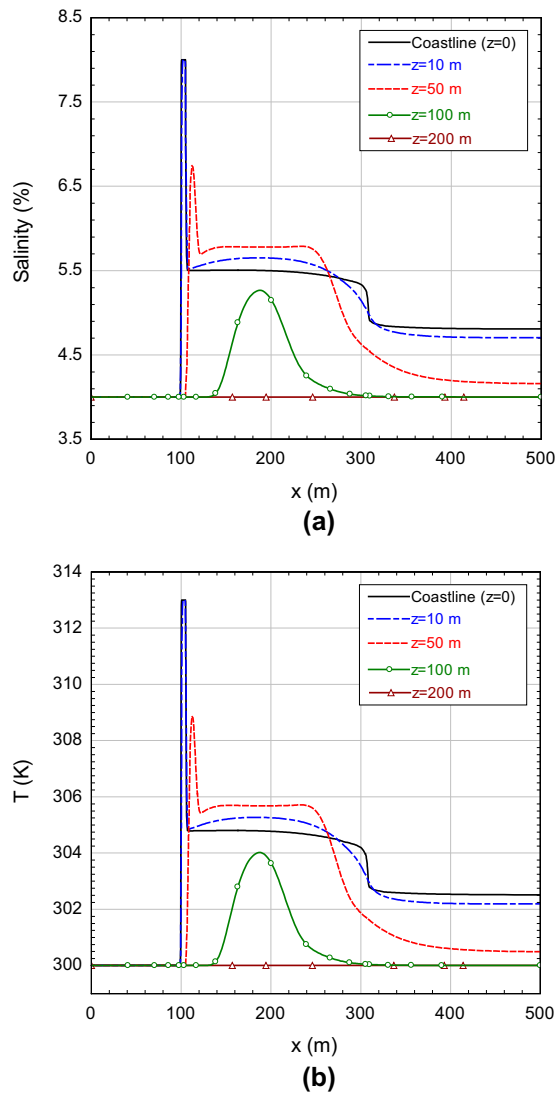

Fig. 5. Salinity (a) and temperature (b) profiles for $u_0 = 0.05$ m/s at different transversal locations ($z = 0$, $z = 10$ m, $z = 50$ m, $z = 100$ m and $z = 200$ m).

The sea currents have a clear impact on the flow, thermal, and mass fields. The discharged plume is deflected towards the coast leading to a significant influence on the intake conditions. In fact, the salinity and temperature at the intake are higher than those of the free stream values.

Fig. 3(a), which illustrates the computed salinity distribution at the free surface, reveals that significant dispersion and mixing with the seawater takes place. Other salinity and temperature contours at 2 m depth, not presented here for lack of space, have also been computed and no clear difference between results of the two depths (at the free surface and at 2 m depth) was observed. This is attributed to the kind of boundary conditions applied on the top and bottom of the domain and also to the shallow water conditions.

One can see the fast drop in salinity from 8% to around 6% within a short distance from the discharge. Similar behavior is observed for the isotherms, Fig. 3(b), which also shows that the heat contained in the discharged stream is spread into the region close to the coast.

Such a general behavior can also be understood by the inspection of the variation of the salinity and temperature profiles at different axial locations (Fig. 4). These axial locations refer mainly to the entrance of the domain ($x = 90$ m), the discharge location ($x = 102.5$ m), the intake location ($x = 307.5$ m), and the exit of the domain ($x = 500$ m). Two other intermediate locations at $x = 250$ m and $x = 320$ m are also given. Fig. 4 shows, for example, that the fluid salinity and temperature profiles at the discharge location exhibit a significant variation within a width of 35 m while at the particular axial position of $x = 250$ m, the fluid located very far from the coastline is found to be affected by the brine discharge.

Fig. 5(a) shows salinity profiles at various locations parallel to the coastline. Near the coast ($z = 0$, 10 and 50 m), the influence of discharge is significant: the salinity (temperature) increases sharply at the discharge location, decreases to an intermediate salinity (temperature) after few meters and then decreases again to about 4.7% (303 K) near the intake port location. At $z = 100$ m, different behavior can be observed

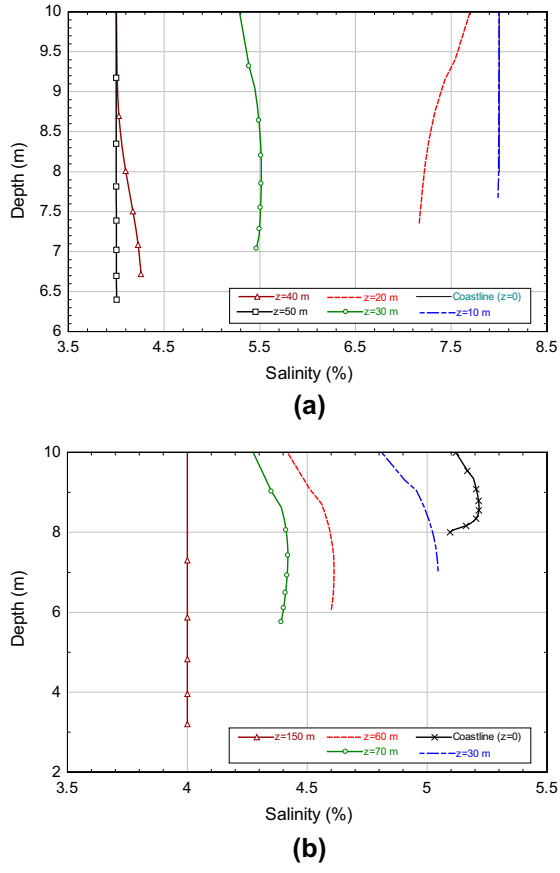

Fig. 6. Distribution of the salinity with depth along the discharge (a) and intake (b) locations.

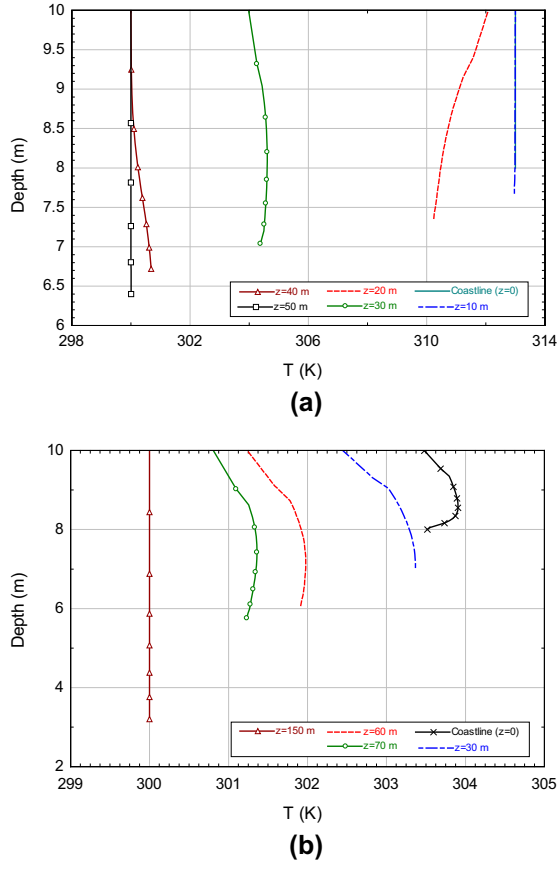

Fig. 7. Distribution of the temperature with depth along the discharge (a) and intake (b) locations.

where the salinity and temperature profiles have the nominal values near the discharge and intake ports but higher values in the intermediate region between $x = 125$ m and $x = 250$ m. This is associated with the recirculation flow described earlier.

Figs. 6 and 7 focus on the vertical variation (depth profiles) of the temperature and salinity at two axial positions; namely, discharge ($x = 102.5$ m) and intake ($x = 307.5$ m) locations. One can recall that in this study, the seabed profile (bed topography) is assumed linear starting with 2 m at the coast to 10 m far from it. The salinity profiles exhibit different but slight variations with the depth along the discharge and intake lines. However, the profiles vary significantly with the transversal (along z) direction. As observed in the previous figures, salinity decreases when moving from the coastline to inside the sea. The temperature profiles, as shown in Fig. 7(b) exhibit similar behavior as that for the concentration.

3.2. Effect of discharge mass flow rate

Fig. 8 illustrate the effect of the mass flow rate of the discharged stream on the heat and mass fields. Three values of mass flow rate equal to 1,000, 3,000, and 5,000 kg/s are considered while the sea current velocity and the discharge salinity are kept constant at 0.05 m/s and 8%, respectively. Although the general patterns of these salinity (temperature) contours are very similar, some differences can be noticed. The

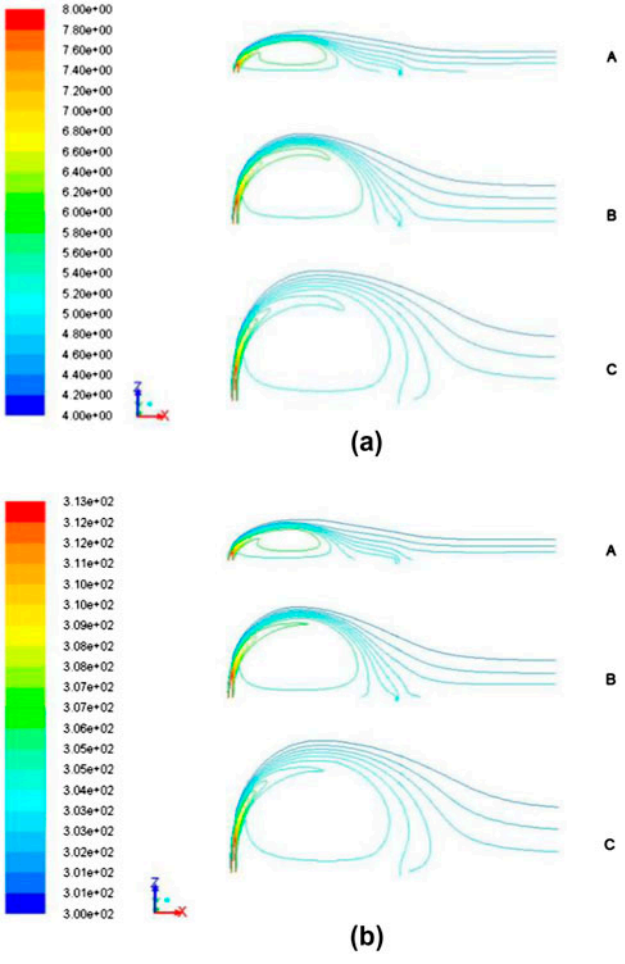

Fig. 8. Effect of the discharge mass flow rate (A-1,000 kg/s; B-3,000 kg/s and C-5,000 kg/s) on the concentration (a) and temperature (b) distribution.

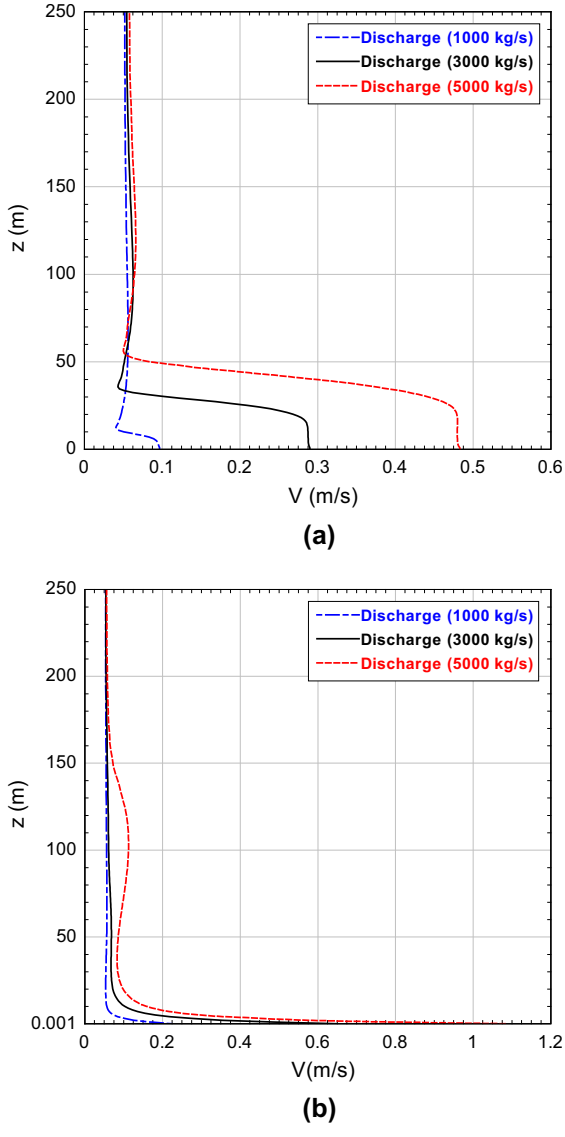

Fig. 9. Variation of the transversal velocity profiles with the discharge mass flow rate at the discharge (a) and intake (b) locations.

deflection of both T and S contours towards the coastline is more pronounced for low discharge mass flow rates. Besides, as the mass flow rate of the discharge stream decreases, the region enveloping the circulation zone is reduced significantly. The dispersion is limited to the region close to the coastline. It is also observed that for the three cases, the intake is affected by the discharge conditions since the hot and saline fluid confined in the discharged plume is deflected towards the coastline in the vicinity of the intake location.

Figs. 9 and 10 depict the variation of the velocity magnitude and salinity profiles along the discharge and intake locations perpendicular to the coastline. They show the affected region on the discharge line increases with the increase of the discharge mass flow rate but remains confined within around 50 m from the coast. The figures also show that although the velocity and salinity at the intake are slightly affected indicating that the mass flow rate of the discharged stream has only slight impact on the values of the velocity and salinity at the intake location; this behavior changes significantly when moving far from the coastline. Thus, increasing the discharge mass flow rate increases significantly the size of the affected region. It is seen for example that when the discharge mass flow rate equals 5,000 kg/s, the salinity remains above the nominal value even at $z = 120$ m. Similar behavior characterizes the temperature profiles.

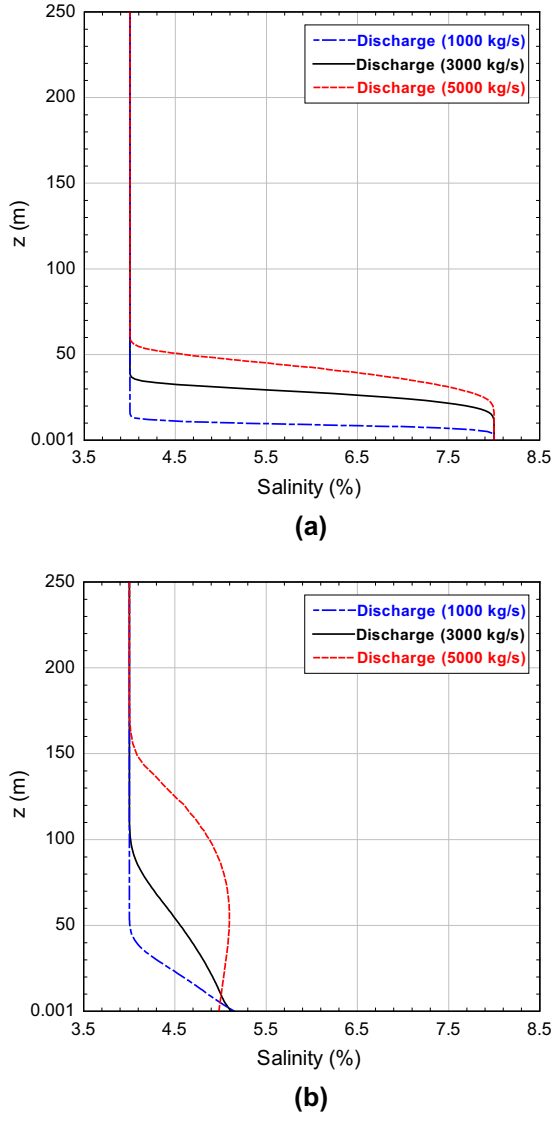

Fig. 10. Variation of the transversal salinity profiles with the discharge mass flow rate at the discharge (a) and intake (b) locations.

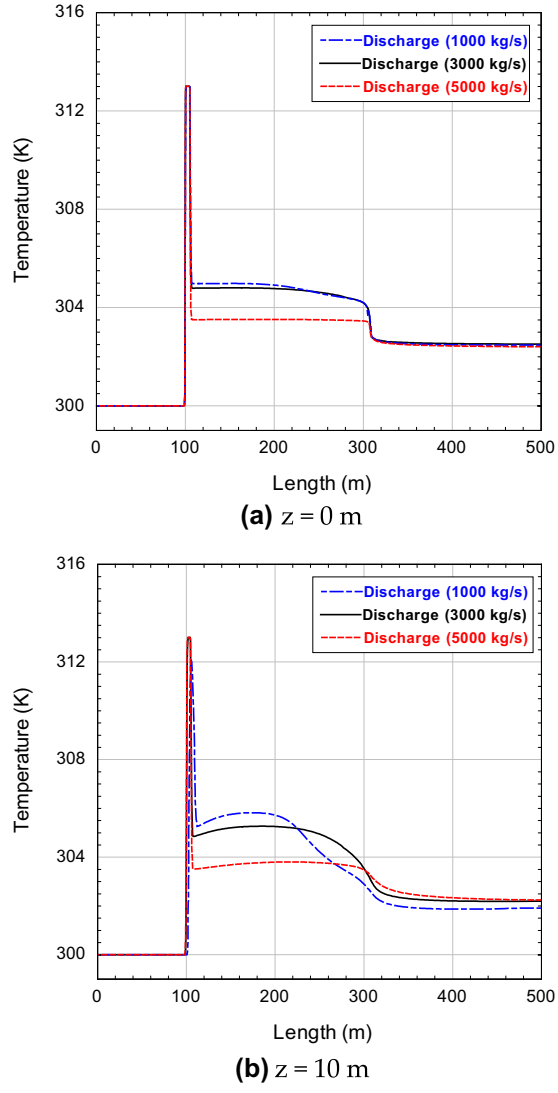

Fig. 11. Temperature profiles at four locations parallel to the coastline (a) $z = 0$ m, (b) $z = 10$ m, (c) $z = 50$ m, and (d) $x = 100$ m.

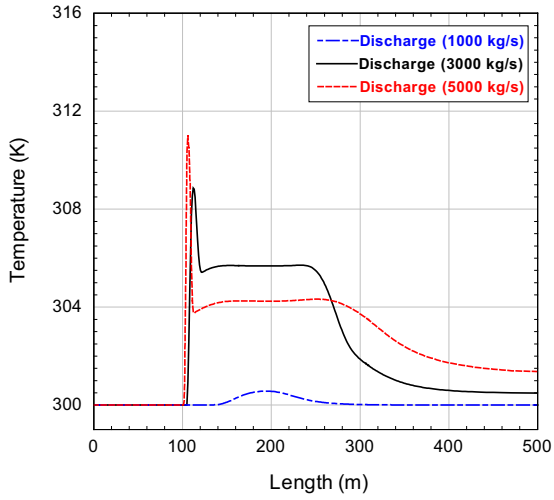

(c) z = 50 m

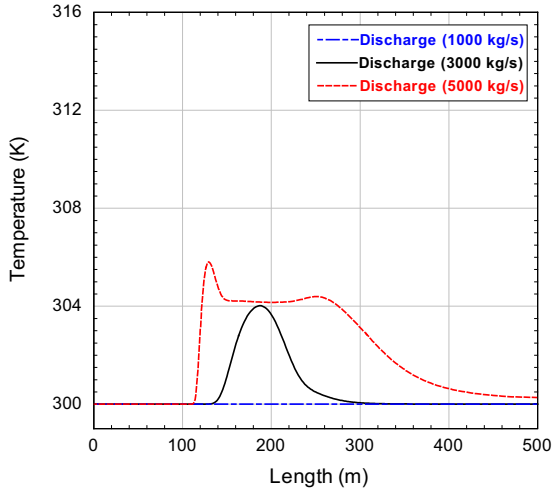

(d) z = 100 m

Fig. 11. (*Continued*)

Fig. 11 shows the variations of the temperature profiles at four locations parallel to the coast line ($z = 0$ m, $z = 10$ m, $z = 50$ m and $x = 100$ m). For low discharge mass flow rates, the influence of the brine discharge is limited to the thin region very close to the coastline. The water temperature increases sharply at the discharge location, decreases to an intermediate salinity after few meters and then decreases again near the intake port location. For higher mass flow rates, the water located even far from the coastline is found to be influenced: its temperature is higher that the nominal temperature of 300 K. One can notice that for all these cases of Fig. 11, the excess temperature, except in the very limited region along the line at the discharge port, remains lower than 6.5 K. The salinity profiles exhibit similar behavior.

Table 3
Temperature and salinity values at the intake for the different cases

Discharge mass flow rate (kg/s)	Intake salinity (%)	Intake temperature (K)
1,000	5.15	304
3,000	5.12	303
5,000	4.98	303

An important parameter on which the brine discharge studies focus concerns the values of the problem variables such as the temperature, salinity, and velocity at the intake ports. Table 3 summarizes the fluid salinity and temperature at the intake port for different mass flow rates. The intake temperature and salinity are always higher than the nominal values (i.e. 300 K and 4%, respectively). For example, for the salinity field, the excess can be as high as 29% of the nominal value.

Finally, it is of interest to note that Al-Sanea [16] studied a similar problem by solving the momentum and species equations using the depth-integrated approach and constant fluid properties. The physical domain considered is larger than the present one. The width and length were taken as 500 and 1,000 m, respectively. The salinity contours the author obtained have the same patterns as those of the present 3D configuration. The author found, for the case of high mass flow rate of 6,000 kg/s, a salinity of 4.9% at the intake port.

4. Conclusions

The problem of brine discharge into sea was studied numerically in this work. A model for the heat and brine dispersion in the vicinity of discharge and intake ports was developed and results were analyzed and compared. The model considered the 3D equations. The flow was taken turbulent and the fluid properties were considered variable with salinity and temperature. The results were expressed in terms of streamlines, isotherms, and salinity contours as well as velocity, temperature, and salinity profiles. These results gave the excess temperature and salinity relative to the nominal values of the free stream. Effect of the discharge mass flow rate on patterns of temperature and salinity contours was presented and analyzed.

As a general picture of the problem under study, one can describe that the physical domain is divided in two regions. The first region, located in the vicinity of the discharge and intake ports, is characterized by

large variations of the temperature and the salinity values due to the recirculating flow structure. The second region, far from the discharge and intake ports, envelops the first region with the recirculation zone and extends to the entry and exit regions of the physical domain. Increasing the discharge mass flow rate increases significantly the size of the affected region. The variation of the temperature and salinity with depth is found to be negligible. It is also observed that for different cases of simulations undertaken in this study, the intake is always affected by the discharge conditions since the hot and saline fluid confined in the discharged plume is deflected towards the coastline in the vicinity of the intake location.

Acknowledgments

The authors would like to thank the National Plan for Science & Technology (NPST) program and King Saud University (KSU) for funding the research reported in this paper through Project Number (08-ENV405-2).

References

[1] T. Bleninger, G.H. Jirka, Environmental Planning, Prediction and Management of Brine Discharges from Desalination Plants, Final Report, Middle East Desalination Research Center, MEDRC Project: 07-AS-003, December, Muscat, Oman, 2010, p. 237.
[2] M. Ahmed, W.H. Shayya, D. Hoey, A. Mahendran, R. Morris, J. Al-Handaly, Use of evaporation ponds for brine disposal in desalination plants, Desalination 130 (2000) 155–168.
[3] R. Danoun, Desalination Plants: Potential Impacts of Brine Discharge on Marine Life, Final Project University of Sydney, Sydney, 2007, p. 55.
[4] I. Al Mutaz, Environmental impact of seawater desalination plants, Environ. Monit. Assess. 16 (1991) 75–84.
[5] P.K. Abdul Azis, I. Al-Tisan, M. Al-Daili, T.N. Green, A. Dalvi, M.A. Javeed, M.A. Javeed, Effects of environment on source water for desalination plants on the eastern coast of Saudi Arabia, Desalination 132 (2000) 29–40.
[6] T. Hoepner, A procedure for environmental impact assessments (EIA) for seawater desalination plants, Desalination 124 (1999) 1–12.
[7] I. Alameddine, M. El-Fadel, Brine discharge from desalination plants: A modeling approach to an optimized outfall design, Desalination 214 (2007) 241–260.
[8] I. Muñoz, A.R. Fernández-Alba, Reducing the environmental impacts of reverse osmosis desalination by using brackish groundwater resources, Water Res. 42 (2008) 801–811.
[9] C. Sommariva, H. Hogg, K. Callister, Environmental impact of seawater desalination: Relations between improvement in efficiency and environmental impact, Desalination 167 (2004) 439–444.
[10] T. Bleninger, A. Niepelt, G. Jerka, Brine Discharge Calculator, European Desalination Society Conference Paper BD 18, May 17–20, Baden Baden, Germany, 2009.
[11] T. Bleninger, Coupled 3D Hydrodynamic Models for Submarine Outfalls: Environmental Hydraulic Design and Control of Multiport Diffusers, University of Karlsruhe, Karlsruhe, 2006.
[12] J. Kuipers, C.B. Vreugdenhil, Calculations of Two-dimensional Horizontal Flow, Report S 163, Part I, Delft Hydraulics Lab, Netherlands, 1973.
[13] D.B. Spalding, Transfer of Heat in Rivers, Bays, Lakes and Estuaries, THIRBLE Report No. HTS/75/4, Department of Mechanical Engineering, Imperial College of Science and Technology, London, 1975.
[14] W. Rodi, Turbulence Models and Their Application in Hydraulics—A State of the Art Review, Report No. SFB 80/T/127, University of Karlsruhe, Germany, 1978.
[15] S.A. Al-Sanea, Numerical Modeling of Two-dimensional Shallow-water Flows (PhD thesis), Department of Mechanical Engineering, Imperial College of Science and Technology, London, 1982.
[16] S.A. Al-Sanea, Computation of the flow and salinity distribution in the vicinity of discharge and intake ports of a desalination plant, J. King Saud Univ. Eng. Sci., 5(1) (1993) 123–140.
[17] A. Purnalna, H.H. Al-Barwani, M. Al-Lawatia, Modeling dispersion of brine waste discharges from a coastal desalination plant, Desalination 155 (2003) 41–47.
[18] A. Purnama, H.H. Al-Barwani, Some criteria to minimize the impact of brine discharge into the sea, Desalination 171 (2005) 167–172.
[19] D.D. Shao, A.W.K. Law, H.Y. Li, Brine discharges into shallow coastal waters with mean and oscillatory tidal currents. J. Hydro-environ. Res. 2 (2008) 91–97.
[20] A. Purnama, H.H. Al-Barwani, Spreading of brine waste discharges into the Gulf of Oman, Desalination 195 (2006) 26–31.
[21] H.H. Al-Barwani, A. Purnama, Re-assessing the impact of desalination plants brine discharges on eroding beaches, Desalination 204 (2007) 94–101.
[22] R. Doneker, G.H. Jirka, CORMIX-GI systems for mixing zone analysis of brine wastewater disposal, Desalination 139 (2001) 263–274.
[23] D. Malcangio, A.F. Petrillo, Modeling of brine outfall at the planning stage of desalination plants, Desalination 254 (2010) 114–125.
[24] O. Palomar, I. Losada, Impacts of brine discharge on the marine environment. Modelling as a predictive tool, in: Desalination, Trends and Technologies, Chap. 3, 2011, pp. 279–310. Available from: www.intechopen.com.
[25] P. Palomar, J.L. Lara, I.J. Losada, M. Rodrigo, A. Alvárez, Near field brine discharge modeling part 1: Analysis of commercial tools, Desalination 290 (2012) 14–27.
[26] P. Palomar, J.L. Lara, I.J. Losada, Near field brine discharge modeling part 2: Validation of commercial tools, Desalination 290 (2012) 28–-42.
[27] A. Cipollina, A. Bonfiglio, G. Micale, A. Brucato, Dense jet modelling applied to the design of dense effluent diffusers, Desalination 167 (2004) 459–468.

[28] M.E. Abou-Elhaggag, M.H. El-Gamal, M.I. Farouk, Experimental and numerical investigation of desalination plant outfalls in limited disposal areas, J. Environ. Prot. 02 (2011) 828–839.
[29] Á Loya-Fernández, L.M. Ferrero-Vicente, C. Marco-Mendez, E. Martinez-Garcia, J. Zubcoff, J. L. Sanchez-Lizaso, Comparing four mixing zone models with brine discharge measurements from a reverse osmosis desalination plant in Spain, Desalination 286 (2012) 217–224.
[30] C.J. Oliver, M.J. Davidson, R.I. Nokes, Predicting the near field of desalination discharges in a stationary environment, Desalination 309 (2013) 148–155.
[31] Fluent 13. Available from: www.ansys.com.